The Astrophysical Journal, 651:782–790, 2006 November 10

MULTIWAVELENGTH OBSERVATIONS OF THE BL LACERTAE OBJECT PKS 2155−304 WITH *XMM-NEWTON*

Y. H. Zhang,[1] J. M. Bai,[2] S. N. Zhang,[1] A. Treves,[3] L. Maraschi,[4] and A. Celotti[5]

Received 2006 April 12; accepted 2006 July 7

ABSTRACT

The optical/UV and X-ray instruments on board *XMM-Newton* provide an excellent opportunity to perform simultaneous observations of violently variable objects over a broad wavelength range. The UV- and X-ray-bright BL Lac object PKS 2155−304 has been observed repeatedly with *XMM-Newton* about twice per year. In this paper, we present a detailed analysis of the simultaneous multiwavelength variability of the source from optical to X-rays, based on the currently available *XMM-Newton* observations. These observations probed the intraday multiwavelength variability at optical/UV and X-ray wavelengths of the source. The UV variability amplitude is substantially smaller than the X-ray one, and the hardness ratios of the UV to X-rays correlates with the X-ray fluxes: the brighter the source, the flatter the UV/X-ray spectra. On 2000 May 30–31, the UV and X-ray light curves were weakly correlated, while the UV variations followed the X-ray ones with no detectable lags on 2000 November 19–21. On 2001 November 30, the source exhibited a major X-ray flare that was not detected in the optical. The intraday UV and X-ray variability presented here is not similar to the interday UV and X-ray variability obtained from the previous coordinated extensive multiwavelength campaigns on the source, indicating that different "modes" of variability might be operating in PKS 2155−304 on different timescales or from epoch to epoch.

Subject headings: BL Lacertae objects: individual (PKS 2155−304) — galaxies: active — methods: data analysis — ultraviolet: galaxies — X-rays: galaxies

Online material: color figures

1. INTRODUCTION

Rapid and large-amplitude variability has been detected frequently on different timescales across the whole accessible electromagnetic spectrum of blazars (see Ulrich et al. [1997] for a review). The nonthermal continuum emission is almost certainly produced by relativistic particles in a tangled magnetic field, in a relativistic jet closely aligned with the line of sight (e.g., Urry & Padovani 1995). Relativistic beaming therefore plays a crucial role in the observed properties of blazars.

Multiwavelength observations have established that the spectral energy distributions (SEDs) of blazars consist of two rather smooth components in the νF_ν representation. The SED peak energies are most likely luminosity related: the lower the luminosity, the higher the peak energy (e.g., Fossati et al. 1998). For low-luminosity BL Lac objects, such as the well-studied sources Mrk 421, Mrk 501, and PKS 2155−304, the low-energy component typically peaks at UV/soft X-ray bands, and for this reason these sources are usually called high-energy peaked BL Lac objects (HBLs). The primary mechanism for this component is believed to be synchrotron radiation of relativistic electrons. The high-energy component is relatively poorly understood. For HBLs that have been detected at TeV energies, the high-energy component appears to peak in the TeV band, and its origin is probably inverse Compton scattering off soft photons, presumably synchrotron photons within the jet, as envisaged by the synchrotron self-Compton (SSC) process (e.g., Urry & Padovani 1995). However, it is still unknown how the emitting particles are accelerated to energies high enough to produce the observed emission and how the plasma is accelerated to a relativistic bulk velocity.

HBLs are highly variable in the X-rays, as expected from the interpretation that the X-ray emission corresponds to the high-energy tail of the synchrotron component. X-ray observations over the last decade with various X-ray telescopes have revealed a remarkably complicated behavior of the X-ray variability (see Pian [2002] and Zhang [2003] for reviews), which cannot be interpreted by simple models. Flux variations are generally accompanied by spectral changes. The X-ray spectrum typically hardens when the source is brighter. Systematic spectral evolution has been resolved for well-defined flares: the peak of the synchrotron emission shifts to higher energy at higher flux levels (e.g., Fossati et al. 2000; Massaro et al. 2004b; Tanihata et al. 2004). Exceptionally high peak energies of the low-energy component—up to ∼100 keV—were detected in Mrk 501 (Pian et al. 1997; Sambruna et al. 2000).

The correlations and possible time lags of variability in different energy bands are also remarkably complicated. The emission at low X-ray energies generally correlates with that at high energies. However, the maximum of the cross-correlation function (CCF) can occur at substantially different time lags (e.g., Tanihata et al. 2001 for Mrk 501; Zhang et al. 1999 for PKS 2155−304; Ravasio et al. 2004 for Mrk 421). Statistically weaker correlations were also found in several other cases. Lags of about 2 hr derived from the X-ray data gathered with low Earth orbit satellites (*ASCA* and *BeppoSAX*) were questioned by the earlier results inferred from *XMM-Newton* data, mainly on the basis of the fact that the continuous observations of *XMM-Newton* have relatively higher signal-to-noise ratios and temporal resolution than periodically interrupted observations of *ASCA* and *BeppoSAX* (Edelson et al. 2001; Sembay et al. 2002). This claim was disputed by Zhang et al. (2004), who performed detailed Monte

[1] Department of Physics and Tsinghua Center for Astrophysics (THCA), Tsinghua University, Beijing 100084, China; youhong.zhang@mail.tsinghua.edu.cn.

[2] National Astronomical Observatories/Yunnan Observatory, Chinese Academy of Sciences, P.O. Box 110, Kunming, Yunnan 650011, China.

[3] Dipartimento di Scienze, Università degli Studi dell'Insubria, via Valleggio 11, I-22100 Como, Italy.

[4] Osservatorio Astronomico di Brera, via Brera 28, I-20121 Milan, Italy.

[5] International School for Advanced Studies, SISSA/ISAS, via Beirut 2-4, I-34014 Trieste, Italy.

Carlo simulations. The results obtained with *BeppoSAX* and *ASCA* have been supported recently by the finding of lags of ∼1000 s and ∼1 hr in the *XMM-Newton* observations of Mrk 421 and PKS 2155−304 (Ravasio et al. 2004; Zhang et al. 2006).

Recently, using *XMM-Newton* timing mode observations of Mrk 421, Brinkmann et al. (2005) presented a time-resolved cross-correlation analysis between the soft and hard energy bands. They showed that the correlations, with different lags of both signs, change on a characteristic timescale of a few times 10^3 s, in qualitative agreement with previous claims about changes of lags during individual flares (e.g., Zhang et al. 2002). Furthermore, it appears that the lag may be related to the flare duration—the longer the flare duration, the larger the lag (Zhang et al. 2002; Brinkmann et al. 2003)—and to the spectral slope: a steeper slope corresponds to a higher probability that the soft band emission leads the hard one (Zhang et al. 2006). The lags generally become larger, and the correlation weaker, with increasing differences of the compared energy bands (e.g., Zhang et al. 2006; Ravasio et al. 2004). Zhang (2002) also found preliminary evidence that in Mrk 421 the lags become larger with increasing timescale, as typically occurs in X-ray binaries.

By measuring variability correlations, time lags, and spectral variations, simultaneous multiwavelength observations offer the strongest constraints on blazar models: namely, on the processes of particles injection/acceleration and diffusion in the emission region(s), and on the relative location of regions dominating the emission at different energies. The previous coordinated multiwavelength observations of a few bright blazars have revealed quite different variability patterns. For example, the variability around the peaks of the two SED components was well correlated in Mrk 421 (Maraschi et al. 1999), while in PKS 2155−304 the fluxes at different wavelengths were not correlated on the measured timescales (Aharonian et al. 2005b). It is important to probe whether the complex X-ray variability patterns mentioned above can be directly extrapolated to the UV and optical ranges, since the optical/UV/X-ray emissions have a common (synchrotron) origin for HBLs. This diagnostics has to be carried out through simultaneous observations. Unlike other coordinated multiwavelength campaigns that need different telescopes at different sites, the Optical Monitor (OM) and X-ray telescopes on board *XMM-Newton* provide a very rare opportunity to simultaneously monitor variable sources such as blazars from optical to X-rays. *XMM-Newton* is thus particularly apt to study the high-energy part of the synchrotron component of HBLs.

The *International Ultraviolet Explorer* (*IUE*) and *Extreme Ultraviolet Explorer* (*EUVE*) satellites revealed that PKS 2155−304 is the brightest BL Lac object at ultraviolet wavelength (Pian et al. 1997; Marshall et al. 2001 and references therein). This is consistent with the possibility that the synchrotron emission of PKS 2155−304 peaks at EUV or even UV bands, as indicated by the fact that multiepoch X-ray spectral analysis of *BeppoSAX* observations did not reliably find spectral peaks in such bands (Zhang et al. 2002). In contrast, in the other two well-studied HBLs, Mrk 421 and Mrk 501, the synchrotron emission peaks in high-energy X-ray bands (Pian et al. 1998; Fossati et al. 2000; Tanihata et al. 2004; Massaro et al. 2004a). PKS 2155−304 is also very bright in the X-ray (e.g., Zhang et al. 2002), optical (e.g., Zhang & Xie 1996 and references therein), and other lower energy bands dominated by synchrotron emission (e.g., Pesce et al. 1997). PKS 2155−304 has also been detected in the 30 MeV–10 GeV band by EGRET (Vestrand et al. 1995), showing a hard spectrum consistent with an SSC component. This indicates that PKS 2155−304 is a good candidate source of TeV emission. Indeed, the Durham Mark 6 telescopes first detected its very high energy γ-ray emission (Chadwick et al. 1999), recently confirmed by the High Energy Stereoscopic System (HESS) at the 45 σ significance level and still detectable even during the dark periods of the HESS observations (Aharonian et al. 2005a). The brightness of PKS 2155−304 through such a broad energy range makes it one of the best-suited blazars for carrying out multiwavelength observations to test emission mechanisms in detail (e.g., Urry et al. 1997; Mimica et al. 2005) and for possibly distinguishing between leptonic versus hadronic origins of the emission (Aharonian et al. 2005b). The intense monitoring of the source over the last two decades, either as single band or coordinated multiwavelength observations, have revealed complex variability patterns and correlations between different energy bands.

Except for one orbit observation as part of the Guest Observer Program on 2000 November 19–21 (Maraschi et al. 2002), PKS 2155−304 has been repeatedly observed during the other eight orbits of *XMM-Newton* as a calibration source. A detailed temporal analysis of the X-ray data from the first six orbits was presented in Edelson et al. (2001) and Zhang et al. (2005, 2006; hereafter Paper I and Paper II). Foschini et al. (2006) presented average OM magnitudes, X-ray spectral properties, and SEDs using part of these observations. In this paper we present a detailed analysis of the multiwavelength variability from optical to X-rays, using the simultaneous data obtained with OM and pn. The aim is to probe whether the X-ray variability properties of the source can be extended to the optical/UV bands, in order to test in detail the cooling and acceleration behavior of the particle distribution responsible for the synchrotron emission. To our knowledge, the data presented here provide the most intensive simultaneous UV and X-ray monitoring achieved with *XMM-Newton* for a blazar.

In § 2 we present the observations and data reduction; the multiwavelength variability analysis is described in § 3. We compare our results with previous coordinated multiwavelength observations and discuss their physical implications in § 4.

2. THE *XMM-NEWTON* OBSERVATIONS AND DATA REDUCTION

During the observations of PKS 2155−304 over nine orbits, spanning over about 6 yr, from 2000 May to 2005 November, all *XMM-Newton* instruments, i.e., the European Photon Imaging Camera (EPIC) pn, the EPIC Metal Oxide Semiconductor (MOS), the Reflection Grating Spectrometer (RGS), and OM, functioned with various configurations. In this paper, we concentrate on OM and pn data from the first three orbits—i.e., orbits 087, 174, and 362—and present a detailed analysis of multiwavelength variability in the optical/UV and X-ray bands. The OM data from other orbits are not suitable for variability analysis because only one or two images are available for each filter, but they are useful to construct the SEDs with simultaneous X-ray data over a long period. We consider X-ray data, relative to the same orbits as the OM data, only from the pn camera because they are less affected by photon pileup and have higher signal-to-noise ratio with respect to the MOS cameras. All *XMM-Newton* data were processed using the latest *XMM-Newton* Science Analysis System (SAS), version 6.5, and the latest available calibration data. The journal of OM observations and related pn observations of the present analysis is shown in Table 1, where an identification number is allocated to each observation.

The OM exposures were taken in standard imaging mode with different filters. We reduced OM imaging data using the standard `omichain` pipeline. The OM images of orbits 087 and 174 were obtained through UV filters, either UVW2 (2120 Å) or UVW1

TABLE 1
OBSERVATIONAL JOURNAL OF PKS 2155−304 WITH *XMM-Newton*

Orbit	Observation ID[a]	Date	Time (TT)	Detector[b]	Filter	Duration (10 ks)	Exposure (10 ks)	CR[c]
087.....	0124930101 (087-1)	2000 May 30	05:33:33–20:39:17	OM	UVW1	40[d]	0.1[e]	72.7
			10:20:09–20:53:29	pn SW	Medium	3.80	2.66	13.2
	0124930201 (087-2)	2000 May 31	00:34:43–19:20:43	OM	UVW2	50[d]	0.1[e]	8.5
			00:52:59–17:21:38	pn SW	Medium	5.93	4.16	12.9
174.....	0080940401 (174-0)	2000 Nov 19	15:40:50–17:08:57	OM	UVW2	5[d]	0.08[e]	13.1
	0080940101 (174-1)		18:42:13–10:41:33[f]	OM	UVW2	50[d]	0.08[e]	12.4
			19:00:40–10:55:39[f]	pn SW	Thin	5.73	4.02	13.5
	0080940301 (174-2)	2000 Nov 20	12:56:53–04:56:12[f]	OM	UVW2	50[d]	0.08[e]	11.4
			13:15:19–05:25:19[f]	pn SW	Thin	5.82	4.08	11.3
362.....	0124930301 (362-1)	2001 Nov 30	03:48:29–05:16:36	OM	*V*	5[d]	0.08[e]	98.4
			05:21:58–06:50:04	OM	*U*	5[d]	0.08[e]	223.3
			06:55:24–08:23:33	OM	*B*	5[d]	0.08[e]	231.2
			03:12:05–15:30:29	pn TI	Medium	4.32	4.27	28.3

[a] The number in parentheses is the identification number used in the text for the observation.
[b] OM was operated in the standard imaging mode. For pn, SW indicates imaging small window, and TI indicates timing mode.
[c] Background-subtracted source count rate. The energy band is 0.2–0.8 keV for pn imaging mode and 0.6–0.8 keV for pn timing mode.
[d] The total number of OM images.
[e] The exposure time for each OM image.
[f] Next day.

(2910 Å). The source counts were extracted in a circular region with $r = 12$ pixels, and the background counts were subtracted from a concentric annular region between pixels 37 and 42. The optical *U* (3440 Å), *B* (4500 Å), and *V* (5430 Å) filters were used for orbit 362 exposures; again we extracted the source counts in a circular region with $r = 12$ pixels and subtracted the background counts from a concentric annular region between pixels 14 and 25.

For imaging mode of the pn exposures (orbits 087 and 174), the source counts were extracted from an annulus, centered on the peak of source counts, to avoid photon pileup effects. The inner and outer radii of the annulus, determined by using the SAS task `epatplot`, are 10″ and 40″, respectively. The part of the orbit 362 observation (362-1, as identified in Paper II) used here was obtained in timing mode, for which pileup can be neglected. We extracted the source photons from rows $25 \geq \mathrm{RAWX} \leq 42$, centered on the brightest strip of the source. Moreover, we selected only single pixel events (pattern = 0) with quality flag = 0 to further minimize photon pileup effects for both the imaging and timing modes. The high particle background periods were examined by computing the hard ($E > 10$ keV) count rates in full frame of the exposed CCD. We found that the background was low and stable for orbits 174-1 and 362-1, while a few background flares occurred in orbits 087-1, 087-2, and 174-2. As in the following analysis, we mainly focus on the soft X-ray energy band that is the least affected by high particle background; we do not cut out the relatively high background periods. We then extracted the background events from regions least affected by source photons to estimate the fraction of background versus source counts. In the 0.2–0.8 keV (imaging mode) and 0.6–0.8 keV (timing mode) bands, the source count rates are of order ∼1000 times the background ones, and even in the 2.4–10 keV band the background is about 5% of the source count rates. Finally, the background count rates were subtracted.

3. RESULTS

3.1. *Orbit 087*

This observation can be split into two parts. For OM observations, the first part (087-1) consists of 40 images (exposures) obtained with the UVW1 filter, while in the second part (087-2) 50 images were obtained through the UVW2 filter. The exposure time of each image is 1000 s for both filters. This results in an almost continuous coverage of the UV light curve for 087-1 and 087-2, while readout time led to regular unexposed intervals of ∼325 s between any two neighboring points of each light curve. The top left panel of Figure 1 shows the UVW1 (087-1, *gray open circles*) and the UVW2 (087-2, *gray filled circles*) light curves normalized to their respective averages. Given the small difference in wavelength, the normalized UVW1 and UVW2 light curves can be roughly viewed as a single light curve in the same energy band. Both UV light curves show visible variability, but have different behavior. The 087-1 light curve presents a long decaying trend, while the 087-2 one is dominated by two flarelike events.

The pn observations were simultaneous to the OM exposures. Edelson et al. (2001) presented a temporal analysis of the pn observations. They showed that the variability amplitude increased with increasing energy, and the variability between different energy bands correlated with no measurable lags. The correlations tend to become weaker with increasing energy differences, in agreement with the results of Paper II obtained with other pn observations. In order to compare the variability between the X-ray and UV bands, we extracted the pn light curves in three energy bands (see Paper II): i.e., 0.2–0.8 keV (soft), 0.8–2.4 keV (medium), and 2.4–10 keV (hard), and rebinned them over the 1000 s long UV exposure time. The soft 0.2–0.8 keV (*black circles*) light curve, normalized to its average, is also plotted in the top left panel of Figure 1 for a direct comparison with the UV light curve.

The UVW1 light curve did not track the soft X-ray one during the 087-1 interval. The X-ray fluxes increased significantly toward the end of this interval, while there was no evidence for increases of the UVW1 flux at the corresponding period. This is different from the good correlation between the light curves at different X-ray bands. However, the smaller variability and larger scatters in the UVW1 fluxes compared to the X-ray ones, and the lack of X-ray data at the start of this interval and the gap between intervals 087-1 and 087-2, prevent us from deriving any clear correlation between the UVW1 and X-ray light curves. Therefore, in the following we do not discuss this period of observations.

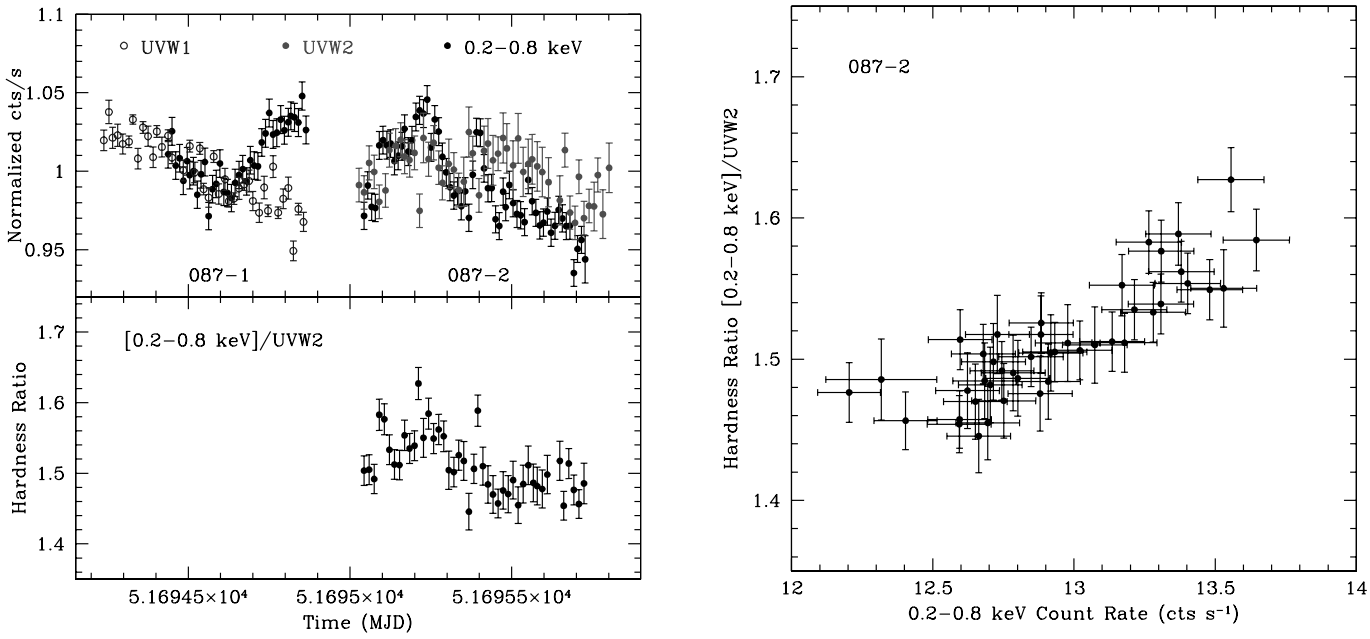

FIG. 1.—Orbit 087 observation. *Left*: The top panel plots the OM UVW1 (*gray open circles*), UVW2 (*gray filled circles*), and pn 0.2–0.8 keV (*black circles*) light curves normalized to their respective averages. The bottom panel plots the variations of the 0.2–0.8 keV/UVW2 HRs with time for the 087-2 interval. *Right*: The correlation between the HRs and the 0.2–0.8 keV count rates for the 087-2 interval. Both the light curves and the HRs are binned in 1000 s. [*See the electronic edition of the Journal for a color version of this figure.*]

During the interval 087-2, the UVW2 light curve appears to follow the soft X-ray one (top left panel of Fig. 1). The left panel of Figure 2 shows the energy dependence of the fractional rms variability amplitude ($F_{\rm var}$) of the UVW2 and X-ray bands. The energy dependence of ($F_{\rm var}$) found in X-rays can be extrapolated to the UVW2 band: the UVW2 variability amplitude is substantially smaller than the X-ray one.

The bottom left panel of Figure 1 shows the temporal evolution of the hardness ratio (HR) of soft X-ray to UVW2 band. As expected, the HR variations generally follow the soft X-ray flux variations given the lower UVW2 variability, indicating that the UV/X-ray spectral changes are mainly related to changes of X-ray intensities. The right panel of Figure 1 reports the HRs as a function of the soft X-ray count rates. Indeed, the two quantities are well correlated—the UV/X-ray spectrum becomes flatter when the X-ray flux is higher. Due to the smaller UVW2 variability, the HRs are indeed weakly correlated with the UVW2 fluxes.

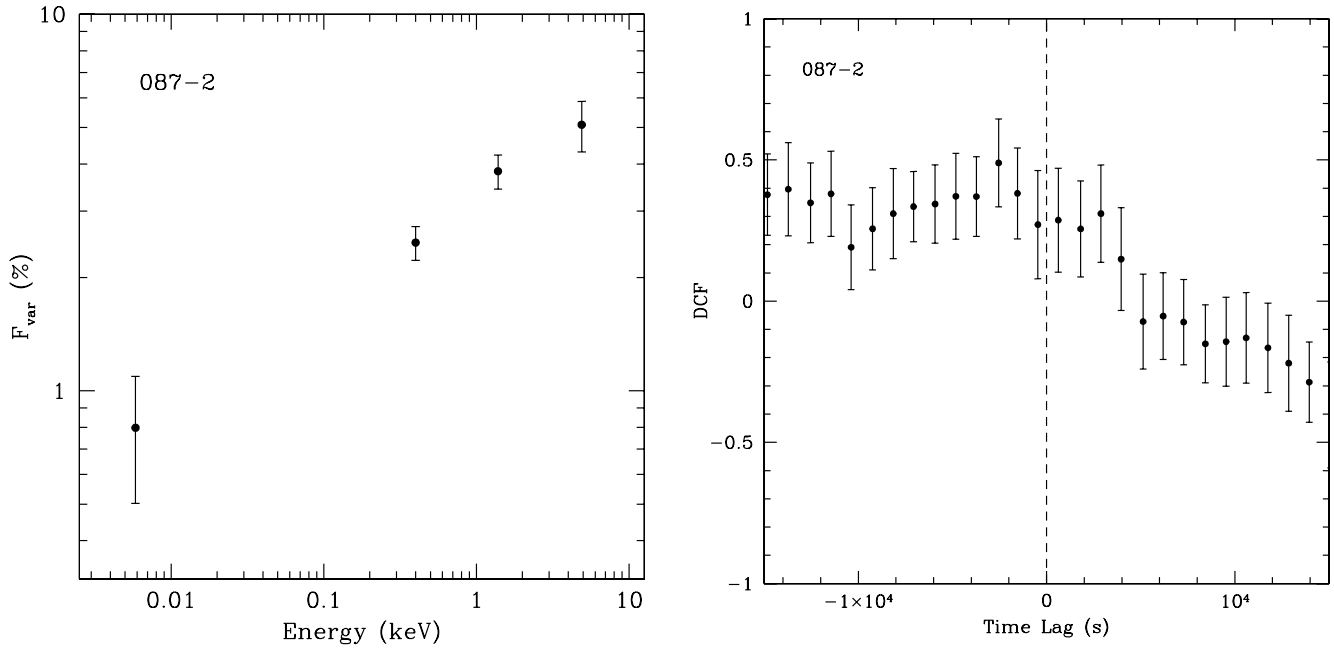

FIG. 2.—Orbit 087-2 observation. *Left*: The fractional rms variability amplitude as a function of energy. *Right*: The central ±15 ks range of the DCF between the UVW2 and 0.2–0.8 keV light curves.

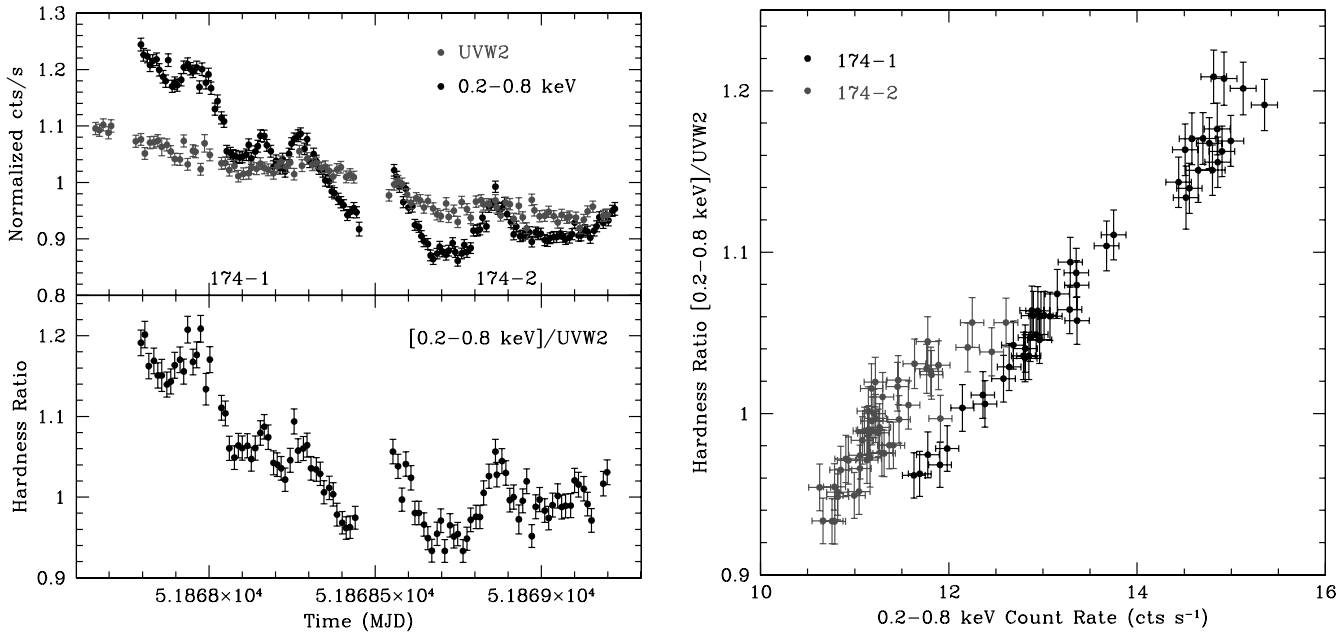

FIG. 3.—Orbit 174 observation. *Left*: The top panel plots the OM UVW2 (*gray circles*) and pn 0.2–0.8 keV (*black circles*) light curves normalized to their respective averages. The bottom panel shows the variations of the 0.2–0.8 keV/UVW2 HRs with time. *Right*: The correlation between the HRs and the 0.2–0.8 keV count rates. Both the light curves and the HRs are binned in 800 s. [*See the electronic edition of the Journal for a color version of this figure.*]

Even though the UVW2 and X-ray light curves are simultaneous, they do not match exactly in time because the OM observing mode is different from the pn one (the latter is counting continuously, while the former is not).[6] Therefore, we calculate the CCF with the discrete correlation function (DCF) method (Edelson & Krolik 1988). The right panel of Figure 2 presents the central 15 ks part of the DCF between the UVW2 and the soft X-ray light curves for 087-2 (a positive lag indicates that the higher energy emission lags the lower energy one). The DCF is strongly asymmetric toward negative lags, indicating that the UVW2 variations may lag the soft X-ray ones. The lack of a clear peak in the DCF prevents us from quantifying any lag.

The DCFs between the UVW2 and medium/hard X-ray bands are similar to that between the UVW2 and soft X-ray band for 087-2. We also calculated DCFs between different X-ray bands. The results are very similar to those presented by Edelson et al. (2001), indicating that the X-ray variations at different energies are correlated with no measurable lags and the correlations tend to become weaker with increasing cross-correlated energy differences.

3.2. *Orbit 174*

The OM images were obtained through the UVW2 filter, and the exposure time was 800 s for each image. The top left panel of Figure 3 plots the UVW2 (*gray circles*) light curve normalized to its average. The OM observations consist of three sections. The first section (174-0) has five exposures without corresponding pn observations. The second (174-1) and the third (174-2) sections, simultaneously monitored with the pn, have 50 exposures each. This yields an almost continuous UVW2 light curve over ~1.5 days. Maraschi et al. (2002) presented the simultaneous UVW2 and X-ray light curves. The UVW2 light curve is obviously variable, dominated by a long decaying trend with superimposed small-amplitude flickers.

The pn light curves (300 s binning) have been presented in Paper II. In order to compare the variability between the UVW2 and X-ray bands, we rebinned the pn light curves over the 800 s long UVW2 exposure time in three energy bands as above and in Paper II. The soft 0.2–0.8 keV (*black circles*) light curve, normalized to its average, is also shown in the top left panel of Figure 3 for a direct comparison with the UVW2 one. The UVW2 light curve follows the X-ray one. However, the UVW2 variability amplitude is significantly smaller than the soft X-ray one, since the overall decrease in the UVW2 light curve is much flatter than that in the soft X-ray one. The fractional rms variability amplitude ($F_{\rm var}$) is 4.5% and 10.8% for the UVW2 and soft X-ray band light curves, respectively. Paper I already showed that the X-ray variability amplitude is larger toward higher energy. The UVW2 variability amplitude is consistent with the extrapolation of the energy-dependent X-ray variability amplitude. This is clearly seen from the top left panel of Figure 4 (*filled circles*), which shows a very good correlation between $F_{\rm var}$ and photon energy. The top left panel of Figure 4 (*open circles*) also shows that the point-to-point fractional rms variability amplitude ($F_{\rm pp}$; see Paper I for its definition) depends on photon energy as well. However, it appears that the ratio of $F_{\rm var}$ to $F_{\rm pp}$ (bottom left panel of Fig. 4) does not depend on energy, suggesting that the slopes of the power spectral density (PSD) are probably energy independent. Therefore, the smaller amplitude of the UVW2 variability is connected to the smaller normalization of the PSD amplitude compared to the X-ray one (see also Paper I).

The bottom left panel of Figure 3 shows the variations of the HRs of the soft X-ray to UVW2 fluxes. The HR variations generally follow the flux variations, especially in the soft X-ray band. This again indicates that the origin of the flux-related UV/X-ray spectral changes is related to the soft X-ray variability as expected from the small UVW2 variability. This behavior is clearly shown in the right panel of Figure 3, which plots the HRs as a function of the soft X-ray count rates. We note a deviation of the

[6] The HRs of the soft X-ray to UVW2 fluxes are obtained from the pn flux most closely matching in time the UVW2 one. In fact, the pn and UVW2 light curves can match exactly in time if one selects the pn exposure bins with the UVW2 exposure time intervals. This, however, reduces the pn observation.

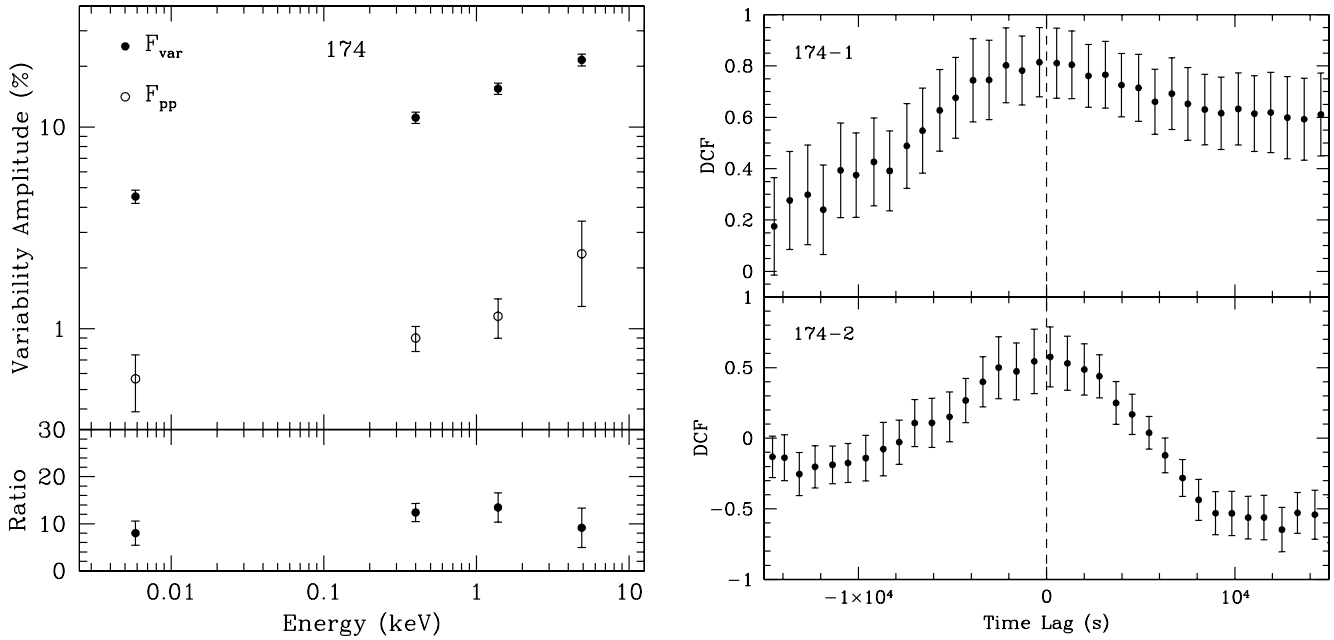

FIG. 4.—Orbit 174 observation. *Left*: The fractional rms variability amplitude as a function of energy over two different timescales (*top*). The upper $F_{\rm var}$ points show the variability amplitude integrated over timescales between the total observational length and ~800 s, and are dominated by variations on timescales comparable to the observation duration because of red noise variability; the lower $F_{\rm pp}$ points indicate the rms deviation between adjacent points (i.e., point-to-point rms), sampling variability on short timescales (~800 s). *Bottom*: The ratio of the two rms spectra, i.e., the ratio spectrum. *Right*: The central ±15 ks range of the DCFs between the UVW2 and the 0.2–0.8 keV light curves.

correlation defined by the interval 174-1 (at high count rates) and 174-2 (at low count rates), showing a harder spectrum for the 174-2 period. This might be interpreted if a less variable and harder emission component contributes more to the observed fluxes when the source is in a faint state.

As in the case of orbit 087, the UVW2 and X-ray light curves do not correspond to each other in time. We calculate the DCFs to examine the correlations between the UV and X-ray emission and determine any possible lags for the 174-1 and 174-2 exposures, respectively. The DCFs between the UVW2 and the soft X-ray light curves are plotted in the right panel of Figure 4. Both of the DCFs peak around zero lag, and the maximum correlation ($r_{\rm max}$) is 0.81 and 0.58 for 174-1 and 174-2 DCF, respectively. This indicates that the UVW2 and soft X-ray variations are correlated, as already suggested by the normalized light curves. However, the two DCFs are not identical. The 174-1 DCF is asymmetric toward positive lags. This indicates that the soft X-ray variability may lag the UVW2 one over the long decaying trend, while they may be simultaneous over short timescales. The DCFs between the UVW2 and the medium/hard X-ray band are more asymmetric toward the positive lags. This behavior is very similar to what is obtained within the X-ray band, as presented in Paper II (left panel of Fig. 6 in that paper). The 174-2 DCF is slightly asymmetric toward negative lags, indicating that the UVW2 and the soft X-ray variations are almost simultaneous. We quantify the possible lag and its significance using Monte Carlo simulations (Peterson et al. 1998). We calculated the probability that the lag is detected as either a negative (soft) or a positive (hard) lag. The results are listed in Table 2. A probability larger than 95% is considered as significant. Both the uncertainties and the probabilities inferred from the simulations show that the lags are consistent with zero for both the 174-1 and 174-2 intervals. However, this result should be taken with caution. The UVW2 light curve of orbit 174 shows a descending trend but no features (peaks or dips) that could be "anchored" to similar features in the X-ray light curve to define a "lag." Therefore, the "zero lag," although formally present, could be induced by a chance coincidence of the two "descending" long-term trends in the UVW2 and X-ray light curves.

3.3. *Orbit 362*

The OM observations were obtained with three different optical (*V*, *B*, *U*) filters. There are five continuous exposures for each filter in time sequence. The exposure time for each image is 800 s. Figure 5 reports, in time order, the *V* (*gray filled circles*), *U* (*gray open circles*), and *B* (*gray filled squares*) light curves normalized to their respective averages. The normalized *V*, *U*, and *B* light curves can be roughly viewed as a single continuous optical light curve given the limited wavelength differences. No pronounced variability is evident in the optical.

The time coverage of the optical light curves partly overlaps with the pn observation. Figure 5 also shows the normalized 0.6–0.8 keV pn light curve (*black circles*) binned over the 800 s

TABLE 2
TIME LAGS AND PROBABILITY

OBSERVATIONS	$r_{\rm max}$	LAG[a] (s) $\tau_{\rm peak}$	LAG[a] (s) $\tau_{\rm cent}$	PROBABILITY[b] (%) $\tau_{\rm peak}$	PROBABILITY[b] (%) $\tau_{\rm cent}$
174-1	0.81	542^{+797}_{-2696}	119^{+438}_{-468}	57.7	71.7
174-2	0.58	194^{+916}_{-1791}	85^{+812}_{-834}	69.8	53.6

[a] The lags are measured with peak ($\tau_{\rm peak}$) and centroid ($\tau_{\rm cent}$) method (see Paper II). The quoted values are the medians of the simulations, and the errors are 68% confidence range with respect to the medians.

[b] The probability that the lag is detected as a hard lag.

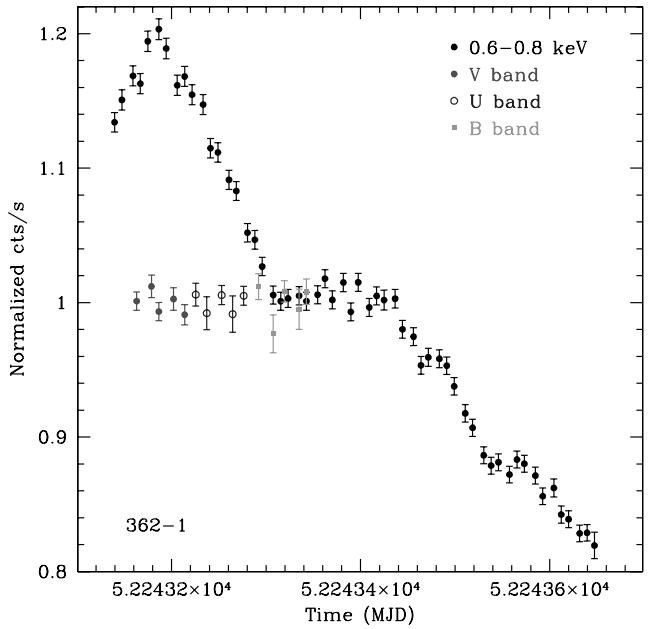

FIG. 5.—Orbit 362 observation. The OM *V*, *U*, *B* (*gray circles*), and pn 0.6–0.8 keV (*black circles*) light curves are normalized to their respective averages. The light curves are binned over 800 s. [*See the electronic edition of the Journal for a color version of this figure.*]

long OM exposure time. While the optical light curves almost cover the period of the prominent X-ray flare, such a flare was not detectable in the optical band.

4. DISCUSSION

In this work we present a detailed multiwavelength timing analysis of PKS 2155−304 with the simultaneous optical/UV and X-ray data obtained during three orbits of observations with *XMM-Newton*. To our best knowledge, these are the most intensive multiwavelength data gathered with different instruments on board *XMM-Newton* for a blazar. In the following we summarize and compare our main findings with those obtained from the previous multiwavelength observations of PKS 2155−304, coordinated with different telescopes, which might be crucial for understanding the complex variability behavior of the source.

4.1. *The XMM-Newton Multiwavelength View*

The correlation between the UV and X-ray light curves of orbit 087 (2000 May 30–31) is not identical to that of seen about half a year later, during orbit 174 (2000 November 19–20). The light curves of orbit 087 appear to be dominated by multiple small-amplitude flarelike events without a long-term trend, while those of orbit 174 follow a long decaying trend, with superimposed short-term timescale events on it. Moreover, it is worth noting that the orbit 174 observation may sample only a decaying phase of a possible major flare. During orbit 174 the UV variations closely follow the X-ray ones with no measurable lag, while during orbit 087 the UV emission weakly correlates with the X-ray one. This difference might be due to the smaller amplitude of variability in orbit 087 than in orbit 174, if indeed small-amplitude variability is not correlated as strong as large-amplitude variability events. Furthermore, the HR analysis shows that the UV/X-ray spectra during orbit 087-2 are significantly harder than those during orbit 174. Nevertheless, in both cases the clear energy dependence of the variability amplitude found in the X-rays can be extrapolated to the UV wavelengths. This is consistent with what would be expected if both bands are dominated by a single synchrotron component. The HR analysis indicates that the UV/X-ray spectra harden with increasing X-ray brightness during both orbits, although with different amplitudes of spectral changes with fluxes. Finally, during orbit 362 (2001 November 30), the source did not show pronounced optical variability, while an intense X-ray flare (more than 40% variability amplitude from minimum to maximum count rates) occurred in the same time interval as the optical observations.

4.2. *Comparison with Previous Multiwavelength Observations*

The *XMM-Newton* multiwavelength observations of PKS 2155−304 revealed that the UV variability may correlate with the X-ray variability with no measurable lags in the two epochs separated by about half a year. This is different from the complex behavior of the correlations between the UV and X-ray variations obtained from the two previous extensive multiwavelength observations of the source in 1991 November and 1994 May, coordinated with *IUE*, *Röntgensatellit* (*ROSAT*), *ASCA*, and ground-based telescopes. During ∼4.5 days of observations in 1991 November, the source showed highly correlated and achromatic variations of small amplitude at optical, UV, and X-ray wavelengths, characterized by multiple flares of roughly the same amplitude and duration. The X-ray variations probably led the UV ones by a couple of hours (Edelson et al. 1995). In contrast, during ∼10 days of the UV observations in 1994 May with *IUE* and *EUVE*, and ∼2 days of the intense X-ray observations with *ASCA* (this campaign also involved observations with *ROSAT* and ground-based radio, infrared, and optical telescopes), the source showed a well-defined flare whose properties strongly depend on photon energy. With increasing wavelengths, the variability amplitude significantly decreased, and the temporal profile of the flare broadened. The variations at different wavelengths were strongly correlated at significant lags, and the lags became larger with larger differences in wavelengths. Specifically, the UV variations lagged the X-ray ones by ∼2 days (Urry et al. 1997).

The first simultaneous multiwavelength campaign involving very high energy (VHE) γ-rays (with HESS) were performed in 2003 October and November (Aharonian et al. 2005b). The observations showed that the source was variable during a low state. However, the VHE γ-ray variations were clearly more intense than those in the X-ray and optical bands, and no correlations between them were detected over the timescales of the observations. The *XMM-Newton* orbit 362 observation may repeat a similar phenomenology on short timescales: a well-resolved major X-ray flare was not followed by a corresponding optical flare.

The *XMM-Newton* observations are superior to the other multiwavelength observations for two reasons. (1) Because *IUE* was a geostationary satellite with 96 minute time resolution required to get a UV spectrum, and *ROSAT* and *ASCA* were low Earth orbit satellites (∼1.6 hr period), the observations with them were characterized by low time resolution and/or periodical gaps. *XMM-Newton* is a high Earth orbit satellite (∼2 day period), so the observations with it can be almost continuous. This implies that the temporal resolution of OM is much higher than that of *IUE*: the typical binning time is ∼15 and ∼96 minutes for OM and *IUE*, respectively. (2) The signal-to-noise ratio of the pn X-ray observations is much higher than those of *ASCA* and *ROSAT*. However, the observation length is ∼1 day for *XMM-Newton* and several days for *IUE*/*ASCA*. Therefore, *XMM-Newton* mostly characterized the intraday multiwavelength variability with the highest temporal resolution, while the other coordinated UV/X-ray observations mainly emphasized extensive interday multiwavelength variations of the source. If the 2 day delay of UV versus X-rays

were present during the *XMM-Newton* observations, it would not have shown up because those were much shorter than 2 days. However, it is also possible that the UV/X-ray correlation and lag may change with time.

4.3. *Physical Implications*

The multiwavelength observations obtained so far showed that the UV and X-ray emission of PKS 2155−304 have consistent variability properties, i.e., the systematic dependence of the variability amplitude on energy, from UV to X-rays, and the similar trends of the UV and X-ray light curves. These similarities/consistences imply a common origin, plausibly synchrotron radiation, for the emission in these bands. However, these observations also showed different patterns of multiwavelength variations, namely, changes of UV/X-ray lags and detailed differences of the UV/X-ray variability on the short timescales. These differences indicate that the constraints on the radiation models would be different at the different energy bands from epoch to epoch, requiring, e.g., changes in the parameters characterizing the emitting region, different mechanisms operating at different times, and/or different dynamical timescales in the UV and X-ray bands.

In the simplistic homogeneous scenario, the synchrotron emission is initiated by a single injection of high-energy electrons in a magnetized volume, followed by energy-dependent cooling: the higher the energy, the faster the cooling. An instantaneous acceleration of high-energy electrons is a representation of such injection. The observed variability properties of the source will depend on the details of the acceleration (e.g., Katarzyński et al. 2005), and the energy that is first emitted will depend on the balance between the acceleration and cooling timescales of the relativistic electrons. Within such a scenario attempts have been made to interpret the remarkably different interband (especially X-ray) time lags detected at different epochs (e.g., Kirk et al. 1998). The energy-dependent amplitude of variability is a natural result of the energy-dependent cooling. When cooling is responsible for the variability behavior, the observed soft lags—i.e., the low-energy variations lagging the high-energy ones—provides a way to estimate the physical parameters of the emitting region (e.g., Zhang et al. 2002).[7] In the observer's frame, we have

$$B\delta^{1/3} = 209.91\left(\frac{1+z}{E_{\rm l}}\right)^{1/3}\left[\frac{1-(E_{\rm l}/E_h)^{1/2}}{\tau_{\rm soft}}\right]^{2/3} \quad {\rm G}, \quad (1)$$

where z is the source's redshift, B is the magnetic field (in gauss), δ is the bulk Doppler factor of the emitting region, and $\tau_{\rm soft}$ is the observed soft lags (in seconds) between the low ($E_{\rm l}$) and high (E_h) energy (in kilo–electron volts), respectively. Equation (1) implies that the larger the lag, the smaller the combination of B and δ. If, as often assumed, δ ($\sim$10) does not change significantly with time, the lag is closely related to B as $B \propto \tau_{\rm soft}^{-2/3}$. In order to be confident about whether B does change significantly with time, one needs proper measurements of the lags with observations obtained at different epochs. However, as we stated in § 4.2, the UV and X-ray light curves obtained with *XMM-Newton* are not comparable with those obtained during previous coordinated multiwavelength observations. In particular, the *XMM-Newton* orbit 174 observations may sample only the decaying phase of a major flare, while the 1994 May campaign caught a complete flare. The UV/X-ray lags measured from these two campaigns may thus have different meanings. Therefore, it is still premature to conclude that the significantly different UV/X-ray lags measured between the two sets of observations indicate intrinsic changes of B.

Furthermore, the interpretation of the observed lags may be very likely affected by, e.g., inhomogeneous emitting region(s), such as in a stratified shock model or in an energy-dependent volume. The achromatic multiwavelength variability showing a quasi periodicity in 1991 November, at odds with the predictions of simple synchrotron emission models, could even have been caused by microlensing by stars in an intervening galaxy (Treves et al. 1997) or associated with helical trajectories of moving knots in a relativistic jet (Urry et al. 1993, 1997).

All the results appear to indicate that the variability behavior observed so far does not provide robust constraints to test or pin down the physical properties of the emitting region. Well-defined major flares, possibly produced by a single variability episode, might still provide the most favorable situation to probe, e.g., any connection between the sign of the lag and the rise and decay of the flux, and any relation between the lag (sign) and the peak energy of the synchrotron emission.

[7] In the following we concentrate on soft lags. A discussion of hard lags (high-energy emission lagging the low-energy one) can be found in our previous work (Zhang 2002; Zhang et al. 2002). In Paper II, we also point out that the probability of detecting a soft lag is higher than detecting a hard lag, as inferred from previous results. This may indicate that the acceleration timescales are usually much shorter than the cooling timescales.

We thank the anonymous referee for constructive suggestions and useful comments. This research is based on observations obtained with *XMM-Newton*, an ESA science mission with instruments and contributions directly funded by ESA Member States and NASA. Y. H. Z. acknowledges Project 10473006, supported by the National Natural Science Foundation of China and the Key Project of Chinese Ministry of Education (106009). J. M. B. acknowledges Project 10573030, supported by the National Natural Science Foundation of China. A. C. acknowledges the Italian MIUR for financial support.

REFERENCES

Aharonian, F., et al. 2005a, A&A, 430, 865
———. 2005b, A&A, 442, 895
Brinkmann, W., Papadakis, I. E., den Herder, J. W. A., & Haberl, F. 2003, A&A, 402, 929
Brinkmann, W., Papadakis, I. E., Raeth, C., Mimica, P., & Haberl, F. 2005, A&A, 443, 397
Chadwick, P. M., et al. 1999, ApJ, 513, 161
Edelson, R. A., Griffiths, G., Markowitz, A., Sembay, S., Turner, M. J. L., & Warwick, R. 2001, ApJ, 554, 274
Edelson, R. A., & Krolik, J. H. 1988, ApJ, 333, 646
Edelson, R. A., et al. 1995, ApJ, 438, 120
Foschini, L., et al. 2006, A&A, 453, 829
Fossati, G., Maraschi, L., Celotti, A., Comastri, A., & Ghisellini, G. 1998, MNRAS, 299, 433
Fossati, G., et al. 2000, ApJ, 541, 166
Katarzyński, K., Ghisellini, G., Tavecchio, F., Maraschi, L., Fossati, G., & Mastichiadis, A. 2005, A&A, 433, 479
Kirk, J. G., Rieger, F., & Mastichiadis, A. 1998, A&A, 333, 452
Maraschi, L., et al. 1999, ApJ, 526, L81
———. 2002, in New Visions of the X-Ray Universe in the *XMM-Newton* and *Chandra* Era, ed. F. Jansen et al. (ESA SP-488), submitted (astro-ph/0202418)
Marshall, H. L., et al. 2001, ApJ, 549, 938
Massaro, E., Perri, M., Giommi, P., & Nesci, R. 2004a, A&A, 413, 489
Massaro, E., Perri, M., Giommi, P., Nesci, R., & Verreecchia, F. 2004b, A&A, 422, 103
Mimica, P., Aloy, M. A., Muller, E., & Brinkmann, W. 2005, A&A, 441, 103
Pesce, J. P., et al. 1997, ApJ, 486, 770

Peterson, B. M., Wanders, I., Horne, K., Collier, S., Alexander, T., Kaspi, S., & Maoz, D. 1998, PASP, 110, 660
Pian, E. 2002, Publ. Astron. Soc. Australia, 19, 49
Pian, E., et al. 1997, ApJ, 486, 784
———. 1998, ApJ, 492, L17
Ravasio, M., Tagliaferri, G., Ghisellini, G., & Tavecchio, F. 2004, A&A, 424, 841
Sambruna, R. M., et al. 2000, ApJ, 538, 127
Sembay, S., Edelson, R. A., Markowitz, A., Griffiths, G., & Turner, M. J. L. 2002, ApJ, 574, 634
Tanihata, C., Kataoka, J., Takahashi, T., & Madejski, G. 2004, ApJ, 601, 759
Tanihata, C., Urry, C. M., Takahashi, T., Kataoka, J., Wagner, S. J., Madejski, G. M., Tashiro, M., & Kouda, M. 2001, ApJ, 563, 569
Treves, A., Rovetti, F., Jetzer, P., & Urry, C. M. 1997, preprint (astro-ph/9702084)
Ulrich, M.-H., Maraschi, L., & Urry, C. M. 1997, ARA&A, 35, 445
Urry, C. M., & Padovani, P. 1995, PASP, 107, 803
Urry, C. M., et al. 1993, ApJ, 411, 614
———. 1997, ApJ, 486, 799
Vestrand, W. T., Stacy, J. G., & Sreekumar, P. 1995, ApJ, 454, L93
Zhang, Y. H. 2002, MNRAS, 337, 609
———. 2003, Publ. Yunnan Obs., 93, 26
Zhang, Y. H., Cagnoni, I., Treves, A., Celotti, A., & Maraschi, L. 2004, ApJ, 605, 98
Zhang, Y. H., Treves, A., Celotti, A., Qin, Y. P., & Bai, J. M. 2005, ApJ, 629, 686 (Paper I)
Zhang, Y. H., Treves, A., Maraschi, L., Bai, J. M., & Liu, F. K. 2006, ApJ, 637, 699 (Paper II)
Zhang, Y. H., & Xie, G. Z. 1996, A&AS, 116, 289
Zhang, Y. H., et al. 1999, ApJ, 527, 719
———. 2002, ApJ, 572, 762